Line tension vector thermodynamics of anisotropic contact lines

Alejandro D. Rey*
Department of Chemical Engineering, McGill University, 3610 University Street, Montreal, Quebec, Canada H3A 2B2
(Received 1 August 2003; published 30 April 2004)

Multiphase materials with intersecting diving surfaces give rise to contact lines. A line tension vector thermodynamics formalism is developed and used to analyze contact line problems in the presence of anisotropy, taking into account two elastic modes: change in contact line length and change in contact line orientation. Using this formalism, the contact line-shape equation is derived, and the renormalization of the line tension due to anisotropy is characterized. The correspondence and analogies between the shape equation for anisotropic surfaces (Herring equation) and the shape equation for contact lines is established. Line energies for nematic liquid crystals, representative of generic anisotropic contact lines, are used to derive a shape equation that takes into account ambient orientation effects. It is found that anisotropic line tension may promote bending and chiral modes to avoid unfavorable orientations of the contact line with respect to the ambient nematic ordering.

DOI: 10.1103/PhysRevE.69.041707 PACS number(s): 61.30.−v

I. INTRODUCTION

The physics of liquid-crystal interfaces is currently an active area of fundamental and applied research [1–6] since many applications of these soft anisotropic mesomorphic materials involve multiphase systems. Orientation phenomena and orientational transitions at surfaces of fixed geometries (hard surfaces) are well characterized experimentally [1–3] and theoretically [4–7]. On the other hand, deforming soft anisotropic nematic interphases are less well-understood. Intersecting interfaces appear in wetting, spreading, floatation, foaming, and fluid-liquid crystal displacement processes and are examples where contact lines are present [8,9]. At present, the understanding and characterization of contact lines formed by the intersection of three or more interfaces that include nematic phases is starting to be developed [10–13]. This paper presents a contribution to the formulation of models of systems displaying nematic-liquid-crystal contact line phases. A typical example is a nematic droplet or lens suspended at the interface between two isotropic fluids. Generalizations to other triple lines, such as those arising at the intersection of solid-isotropic-fluid–nematic-liquid-crystal phases, can be made following the procedure presented in this paper. Since liquid crystals are anisotropic soft materials, elastic anisotropy is present also at interfaces and contact lines. This paper focuses on the role of elastic anisotropy on contact lines. Figure 1 shows a representative schematic of a contact line (C^{cl}) arising from the intersections of three interfaces: α-N, N-β, and α-β. In this paper, N represents a uniaxial nematic liquid crystal, and hence the contact line is anisotropic due to the presence of nematic orientational order defined by the unit vector (director) **n**.

Theories for liquid-crystal statics are classified according to their level of description of nematic order, such as in (i) Landau–de Gennes theory, which describes nematic order using the tensor order parameter, and (ii) the Frank-Oseen theory, which uses the director vector to describe nematic ordering. The tensorial Landau–de Gennes force and torque balance equations of nematic liquid crystals have been presented and used extensively for bulk, surface, and line phases (see, for example, [3,5,10,13–17]). The vectorial Frank-Oseen force and torque balance equations of nematic liquid crystals have also been formulated and used for bulk, surface, and line phases with various degrees of approximations (see, for example, [1,3,6,10,13,14,18]). In this paper, we shall derive a simple vectorial director theory for nematic contact lines, and hence scalar order parameter [14] phenomena are beyond the scope of this paper.

It is useful to briefly consider anisotropy in surface phases. The contribution of anisotropy in interfacial statics is embodied in Herring's equation for capillary pressure p_c [19,20]:

$$-p_c = \underbrace{\gamma(\kappa_1+\kappa_2)}_{\text{area size change}} + \underbrace{\left(\frac{\partial^2\gamma}{\partial\theta_1^2}\kappa_1+\frac{\partial^2\gamma}{\partial\theta_2^2}\kappa_2\right)}_{\text{area rotation}} \tag{1}$$

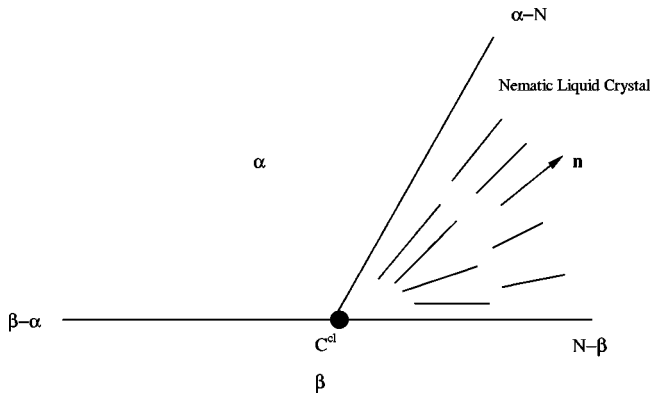

FIG. 1. Schematic of a contact line (C^{cl}) arising from the intersections of three interfaces: α-N, N-β, and α-β. In this paper, N represents a uniaxial nematic rodlike liquid crystal, and hence the contact line is anisotropic due to the presence of nematic orientational order defined by the unit vector (director) **n**. In this case, the contact line is a triple line.

*Email address: alejandro.rey@mcgill.ca

where γ is the surface tension, $\partial^2\gamma/\partial\theta_i^2; i=1,2$ are the second derivatives with respect to surface inclination along the direction of maximum surface energy change, and κ_1 and κ_2 are the surface curvatures. The underlying text shows the physical origin of two contributions: (i) change in surface energy due to changes in the area size (isotropic effect), and (ii) change in surface energy due to area rotation (anisotropic effect). For anisotropic surfaces, the capillary pressure is the divergence of the capillary vector ξ^s [19,20]:

$$p_c=\nabla_s\cdot\boldsymbol{\xi}^S \tag{2}$$

defined by

$$\int \gamma\, dA=\int \boldsymbol{\xi}^S\cdot\mathbf{k}\, dA, \tag{3}$$

where $\mathbf{k}$ is the outward unit normal, and which indicates that for anisotropic surfaces the scalar surface tension is insufficient to describe surface processes since surface energy can also be changed by surface tilting.

Herring's equation is widely used to model capillary phenomena in hard anisotropic surfaces [19,20]. Using surface elastic anchoring energies specific to liquid crystals, previous work showed that the capillary vector and Herring's equation for nematic-liquid-crystal interfaces are [21,22]

$$\boldsymbol{\xi}^S=\gamma\mathbf{k}+(\mathbf{I}-\mathbf{k}\cdot\mathbf{k})\cdot\frac{\partial\gamma}{\partial\mathbf{k}}, \tag{4}$$

$$\begin{aligned}-p_c=&\{\gamma+\gamma''[(\mathbf{n}\cdot\mathbf{e}_1)^2-(\mathbf{n}\cdot\mathbf{k})^2]\}\kappa_1+\{\gamma+\gamma''[(\mathbf{n}\cdot\mathbf{e}_2)^2\\&-(\mathbf{n}\cdot\mathbf{k})^2]\}\kappa_2-\gamma''\{\mathrm{tr}(\mathbf{k}\cdot\mathbf{n})\mathrm{tr}(\nabla_s\cdot\mathbf{n})\\&+\mathrm{tr}[(\mathbf{k}\cdot\mathbf{n})(\nabla_s\cdot\mathbf{n})]\},\end{aligned} \tag{5}$$

where the coefficients of the $\partial^2\gamma/\partial\theta_i^2=\gamma''[(\mathbf{n}\cdot\mathbf{e}_i)^2-(\mathbf{n}\cdot\mathbf{k})^2]$; $i=1,2$ terms are orientation-dependent and where the additional last term is due to director curvature; here γ'' is the anchoring energy, and $\mathbf{e}_i$; $i=1,2$ are the eigenvectors along the principal directions of the surface. The usefulness of capillary vector thermodynamics for nematic interfaces was illustrated in [22]. Given the usefulness of formulating and using vectorial thermodynamics for anisotropic surfaces, it is natural to expect that similar advantages will be found in formulating a vectorial thermodynamics for anisotropic contact lines. In this paper, we derive a line tension vector thermodynamics and show that it provides an efficient path to analyze anisotropic contact line problems.

Anisotropic line tension has been found in Langmuir monolayers [23,24], in crystalline materials [25,26], and in sessile drops supported by anisotropic elastic solids [27]. In Langmuir monolayers, noncircular cardiod-shaped domains arise due to an anisotropic contribution to the contact line [23,24]. It was found that the line tension is a function of chain orientation with respect to the normal to the domain boundary [23]. The evolution of two-dimensional (2D) wormlike clusters on metal surfaces has been characterized using anisotropic line tension [26]. The wetting properties of soft anisotropic solids, such as gels and rubbers, was found to be a function of direction on the surface [27]. A classification of line tensions for 2D and 3D systems based on theoretical and experimental considerations has been presented [27]. Given this evidence, liquid-crystal mesophases are expected to be good candidates to observe line tension anisotropy.

The objectives of this paper are to (i) derive the line vector thermodynamics for anisotropic contact lines and characterize the energy storage modes represented by its components, (ii) use liquid-crystal line energies to derive the nematic line vector thermodynamics, (iii) establish the correspondence between the contact line vector thermodynamics and 1D nematostatics, as given in [13], (iv) derive the shape equation for nematic contact lines, and (v) demonstrate the usefulness of line vector thermodynamics by analyzing contact line-shape transitions.

The organization of this paper is as follows. Section II derives the generalized line tension vector for anisotropic contact lines. Section III derives the line tension vector for nematic contact lines. Section IV establishes the equivalence of the line tension vector and elastic line stress vector for nematic contact lines. Section V derives the shape equation for anisotropic contact lines. Section VI presents an application of the model, and analyzes anchoring-driven shape transitions in nematic contact lines. Section VII presents the conclusions.

II. THE LINE TENSION VECTOR FOR ANISOTROPIC CONTACT LINES

To describe the geometry of a contact line C^{cl}, we use the Frenet-Serret formulas. The principal geometric frame is $(\mathbf{t},\mathbf{p},\mathbf{b})$, where $\mathbf{t}=\mathbf{p}\times\mathbf{b}$ is the unit tangent, $\mathbf{p}=\mathbf{b}\times\mathbf{t}$ is the unit principal normal, and $\mathbf{b}=\mathbf{t}\times\mathbf{p}$ is the binormal unit vector. Representing the contact line by $\mathbf{r}=\mathbf{r}(s)$, the curvature κ and the torsion τ are

$$\frac{d}{ds}\begin{bmatrix}\mathbf{t}\\ \mathbf{p}\\ \mathbf{b}\end{bmatrix}=\begin{bmatrix}0 & \kappa & 0\\ -\kappa & 0 & \tau\\ 0 & -\tau & 0\end{bmatrix}\begin{bmatrix}\mathbf{t}\\ \mathbf{p}\\ \mathbf{b}\end{bmatrix}. \tag{6}$$

The unit line diad is $\mathbf{I}_\ell=\mathbf{tt}$ and the cross-section projection tensor is $\mathbf{I}_c=\mathbf{I}-\mathbf{I}_\ell$. The line gradient operator is $\nabla_\ell(\cdot)=\mathbf{I}_\ell\cdot\nabla(\cdot)$. The divergence of the unit dyad is $\nabla_\ell\cdot\mathbf{I}_\ell=\kappa\mathbf{p}$. The linear curvature dyadic β_ℓ is given by

$$\beta_\ell=-\nabla_\ell\cdot\mathbf{p}=\kappa\mathbf{tt} \tag{7}$$

and the line curvature κ by

$$\kappa=-\nabla_\ell\cdot\mathbf{p}=\mathbf{I}_\ell:\beta_\ell=-\mathbf{I}_\ell:\nabla_\ell\cdot\mathbf{p}. \tag{8}$$

Next we derive the contact line vector. For anisotropic materials, the line free-energy density χ is a function of the line unit tangent $\mathbf{t}$: $\chi(\mathbf{t})$. The line tension vector $\boldsymbol{\xi}(\mathbf{t})$ is defined by the gradient of the scalar field $r\chi$,

$$\xi(\mathbf{t})=\nabla(r\chi),\quad \mathbf{r}=r\mathbf{t}, \tag{9}$$

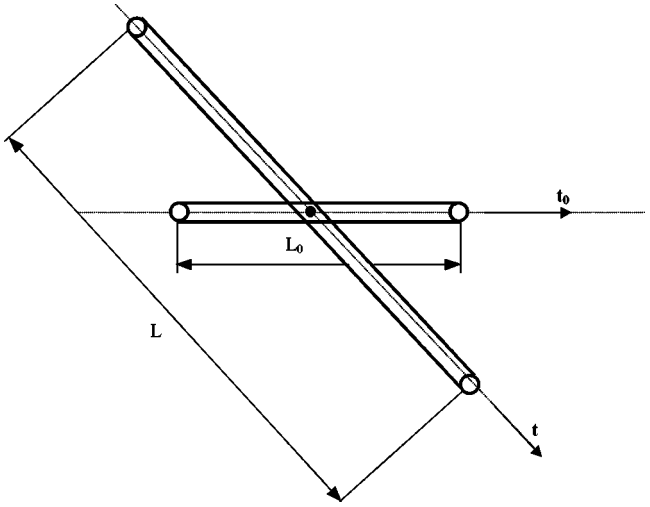

FIG. 2. Schematic of a contact line element of length $L_o = \mathbf{L}_o \cdot \mathbf{t}_o$ and line unit tangent $\mathbf{t}_o$ that undergoes an expansion to L and a rotation to $\mathbf{t}$. Since the line energy density $\chi(\mathbf{t})$ is a function of $\mathbf{t}$, the total line energy X of the contact line can be increased by the stretching of its length L_o and by rotation of its unit tangent $\mathbf{t}_o$.

where r is the magnitude of line position vector $\mathbf{r}$. Noting that $\chi(\mathbf{t})$, the gradient of $r\chi$ yields

$$d(r\chi) = \nabla(r\chi) \cdot d\mathbf{r},$$

$$r d\chi + \chi dr = \boldsymbol{\xi} \cdot d(r\mathbf{t}) = r\boldsymbol{\xi} \cdot d\mathbf{t} + \boldsymbol{\xi} \cdot \mathbf{t} dr. \tag{10}$$

Since $\boldsymbol{\xi} \cdot d\mathbf{t} = \boldsymbol{\xi}_\perp \cdot d\mathbf{t}$ and $\boldsymbol{\xi} \cdot \mathbf{t} = \boldsymbol{\xi}_\parallel$, it follows by comparing the coefficients of dr and dt that

$$\boldsymbol{\xi}_\parallel = \boldsymbol{\xi} \cdot \mathbf{tt} = \chi \mathbf{t}, \tag{11a}$$

$$d\chi = \boldsymbol{\xi}_\perp \cdot d\mathbf{t}. \tag{11b}$$

Dividing Eq. (11b) by $d\theta$, it follows that

$$\boldsymbol{\xi} \cdot \frac{d\mathbf{t}}{d\theta} = \frac{d\chi}{d\theta}, \tag{12}$$

where $d\theta = |d\mathbf{t}|$ is a small rotation angle. Since the corresponding unit normal vector is given by $\mathbf{p} = d\mathbf{t}/d\theta$, then it follows that $\boldsymbol{\xi}_\perp = \boldsymbol{\xi} \cdot \mathbf{p} = d\chi/d\theta$. The selected normal component of the line tension vector $\boldsymbol{\xi}$ is the one that maximizes the increase of surface energy with rotation, and hence

$$\boldsymbol{\xi}_\perp = \boldsymbol{\xi} \cdot \mathbf{I}_c = \left(\frac{d\chi}{d\theta} \right)_{\max} \mathbf{p}_o, \tag{13}$$

where $\mathbf{p}_o$ is the unit normal vector along which $d\chi/d\theta$ has the maximum rate of increase. For anisotropic contact lines, there is a principal anisotropy coordinate frame $(\mathbf{p}_o, \mathbf{b}_o)$, and the rotation of the unit line tangent $\mathbf{t}$ around $\mathbf{b}_o$ produces the maximum increase in surface energy. The principal anisotropy frame $(\mathbf{p}_o, \mathbf{b}_o)$ on the plane normal to $\mathbf{t}$ is selected by the main anisotropic axes of the surface. Anisotropic lines can change line energy by dilation and by rotation. Figure 2 shows an element of length $L_o = \mathbf{L}_o \cdot \mathbf{t}_o$ and line unit tangent

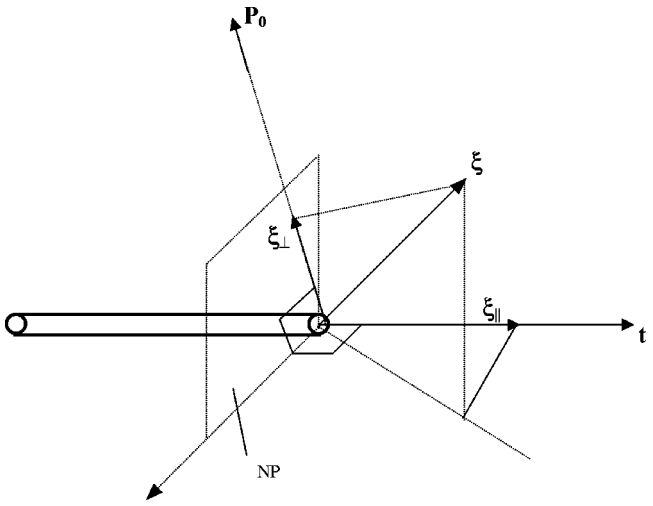

FIG. 3. Definition and geometry of the contact line vector $\boldsymbol{\xi}$ for anisotropic contact lines. Schematic of a segment of the contact line, the contact line vector $\boldsymbol{\xi}$ and its components, the principal anisotropy frame $(\mathbf{p}_o, \mathbf{b}_o)$, and the normal plane (NP) to the unit tangent $\mathbf{t}$. The projection of the line vector $\boldsymbol{\xi}$ on the NP defines the principal anisotropy frame $(\mathbf{p}_o, \mathbf{b}_o)$.

$\mathbf{t}_o$ of the contact line that undergoes an expansion to L and rotation to $\mathbf{t}$. Since the line energy density is a function of $\mathbf{t}$, $\chi(\mathbf{t})$, the total line energy X of the contact line can be increased by expansion and by rotation of $\mathbf{t}$. Figure 3 shows a segment of the contact line, the components of the contact line vector $\boldsymbol{\xi}$, their magnitudes, the principal anisotropy frame $(\mathbf{p}_o, \mathbf{b}_o)$, and the normal plane (NP) to the unit tangent $\mathbf{t}$. The principal anisotropy frame $(\mathbf{p}_o, \mathbf{b}_o)$ defines the NP. Figure 4 shows a schematic of the capillarity vectors $\boldsymbol{\xi}$ and $-\boldsymbol{\xi}$, the normal $-\boldsymbol{\xi}_\perp$ and tangential $-\boldsymbol{\xi}_\parallel$ components of $-\boldsymbol{\xi}$, acting on a point of the contact line, the NP, and the unit tangent vector $\mathbf{t}$. The vector $-\boldsymbol{\xi}$ represents the line force acting on the line vector $\mathbf{L} = L\mathbf{t}$ tending to rotate $(-\boldsymbol{\xi}_\perp)$ and

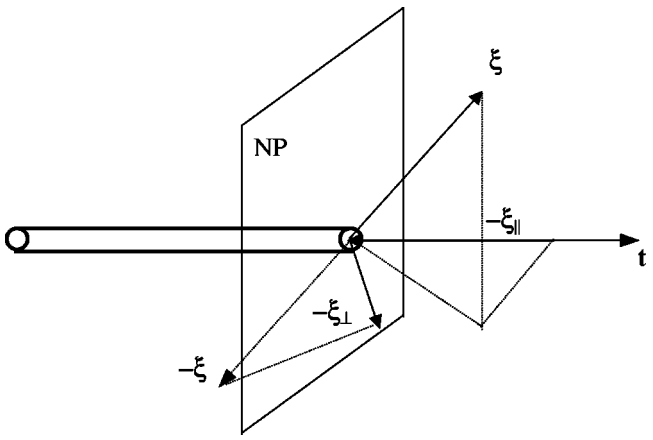

FIG. 4. Schematic of the capillarity vectors $\boldsymbol{\xi}$ and $-\boldsymbol{\xi}$, the normal $-\boldsymbol{\xi}_\perp$ and tangential $-\boldsymbol{\xi}_\parallel$ components of $-\boldsymbol{\xi}$, acting on a point of the contact line, the normal plane (NP), and the unit tangent vector $\mathbf{t}$. The vector $-\boldsymbol{\xi}$ represents the line force acting on the line vector $\mathbf{L} = L\mathbf{t}$ tending to rotate $(-\boldsymbol{\xi}_\perp)$ and shrink $(-\boldsymbol{\xi}_\parallel)$ the line. For isotropic surfaces, $\boldsymbol{\xi}_\perp = \mathbf{0}$ and no rotational effects appear.

shrink ($-\boldsymbol{\xi}_{\parallel}$) the contact line. For isotropic surfaces, $\boldsymbol{\xi}_{\perp}=\mathbf{0}$ and no rotational effects appear.

Finally, the torque $\boldsymbol{\sigma}$ acting on the unit tangent $\mathbf{t}$ is given by

$$\boldsymbol{\sigma}=\boldsymbol{\xi}\times\mathbf{t}=\mathbf{t}\times(-\boldsymbol{\xi}_{\perp})=\left(-\frac{d\chi}{d\theta}\right)_{\max}(\mathbf{t}\times\mathbf{p}_o)\equiv\left(-\frac{d\chi}{d\theta}\right)_{\max}\mathbf{b}_o. \tag{14}$$

For isotropic lines, the torque is zero.

III. THE LINE TENSION VECTOR FOR NEMATIC CONTACT LINES

As mentioned above, for a nematic-liquid-crystal contact line, the nematic orientational order is defined by the three-component orientation unit vector mentioned above, $\mathbf{n}=\mathbf{n}(\mathbf{r})$, where $\mathbf{n}\cdot\mathbf{n}=1$. The tangential and normal components of the director field are $\mathbf{n}_{\parallel}=\mathbf{tt}\cdot\mathbf{n}$ and $\mathbf{n}_{\perp}=(\mathbf{I}-\mathbf{tt})\cdot\mathbf{n}$. The total elastic free energy of the contact line is

$$X=\int\chi ds=\chi_0\int ds+\frac{\chi_2}{2}\int\left(\frac{d\mathbf{r}}{ds}\cdot\mathbf{n}(\mathbf{r}(s))\right)^2 ds, \tag{15a}$$

$$\chi(\mathbf{n}\cdot\mathbf{t},T)=\chi_o(T)+\chi_{an}(\mathbf{n}\cdot\mathbf{t},T), \tag{15b}$$

$$\chi_{an}(\mathbf{n}\cdot\mathbf{t},T)=\frac{\chi_2}{2}(T)\ \ [\mathbf{n}\cdot\mathbf{t}]^2, \tag{15c}$$

where χ_o is the isotropic contribution, χ_{an} is the anisotropic anchoring energy contribution, $\chi_2(T)$ is the anchoring coefficient, and T is the temperature. The anisotropic anchoring energy has been used to describe elastic (i.e., flexible polymers) lines embedded in a nematic matrix [28]. More general models containing line gradient terms have been proposed [13] but are beyond the scope of this paper. In this paper, we shall assume that $\chi>0$, $\chi_o>0$, and the admissible values of the anchoring coefficient then are $-2\chi_0<\chi_2$.

To derive the nematic line tension vector $\boldsymbol{\xi}$, we use Eq. (9):

$$\boldsymbol{\xi}(\mathbf{n},\mathbf{t})=\boldsymbol{\nabla}(\mathbf{r}\chi(\mathbf{t})),\mathbf{r}=\mathbf{rt}, \tag{16}$$

where the director $\mathbf{n}$ is kept constant and hence $\chi(\mathbf{t})$. Computing the gradient of the scalar $\mathbf{r}\chi$, using $r=r(\mathbf{r},\mathbf{t})$ and $\mathbf{t}=\mathbf{t}(\mathbf{r})$, gives

$$\boldsymbol{\xi}(\mathbf{n},\mathbf{t})=\boldsymbol{\nabla}(\mathbf{r}\chi(\mathbf{t}))=\chi\frac{\partial r}{\partial\mathbf{r}}+r\frac{d\chi}{d\mathbf{r}}=\chi\mathbf{t}+\mathbf{I}_c\cdot\frac{d\chi}{d\mathbf{t}}. \tag{17}$$

Thus the components of the line tension vector for nematic contact lines are

$$\boldsymbol{\xi}_{\parallel}=\chi\mathbf{t}; \tag{18a}$$

$$\boldsymbol{\xi}_{\perp}=\mathbf{I}_c\cdot\frac{d\chi}{d\mathbf{t}}=(\mathbf{I}_c\cdot\mathbf{n})\frac{d\chi}{d(\mathbf{n}\cdot\mathbf{t})}=\chi'\mathbf{n}_{\perp}, \tag{18b}$$

where $\chi'=d\chi/d(\mathbf{n}\cdot\mathbf{t})$. To put $\boldsymbol{\xi}_{\perp}$ in the general form of anisotropic contact lines [see Eq. (13)], we let θ be the angle between the unit tangent $\mathbf{t}$ and the director $\mathbf{n}$, and get

$$\boldsymbol{\xi}_{\perp}=\mathbf{I}_c\cdot\frac{\partial\gamma}{\partial\mathbf{t}}=\left(\frac{d\chi}{d\theta}\right)_{\max}\mathbf{p}_o, \tag{19a}$$

$$\left(\frac{d\chi}{d\theta}\right)_{\max}=\left(-\frac{d\chi}{d\theta}\right), \tag{19b}$$

$$\mathbf{p}_o=\frac{\mathbf{n}_{\perp}}{|\mathbf{n}_{\perp}|}. \tag{19c}$$

Thus the maximum rate of increase of χ is just $-d\chi/d\theta$, and the selected normal vector $\mathbf{p}_o$ is the normal unit vector along the projection of the director on the cross-sectional plane: $\mathbf{p}_o=\mathbf{n}_{\perp}/|\mathbf{n}_{\perp}|$. In nematic lines, the principal anisotropy frame ($\mathbf{p}_o$, $\mathbf{b}_o=\mathbf{t}\times\mathbf{p}_o$) is defined by the intersection of the **t**-**n** plane and the cross-sectional surface (NP), and in that frame the line tension vector reads

$$\boldsymbol{\xi}=\left(\chi,\mathbf{p}_o\cdot\frac{\partial\chi}{\partial\mathbf{t}},0\right). \tag{20}$$

Thus nematic contact lines may decrease the line energy by contraction or by rotation of the unit tangent around an axis that is perpendicular to the projection of the director on the cross-sectional surface. The nematic contact line behavior is isotropic only if

$$\boldsymbol{\xi}_{\perp}=\chi'\mathbf{n}_{\perp}=\mathbf{0}, \tag{21}$$

which is possible when $\mathbf{n}_{\perp}=\mathbf{0}$ or when $\chi'=0$. When $\mathbf{n}\|\mathbf{t}$, the contact line behavior is isotropic. The special directors $\mathbf{n}^*$ corresponding to the stable extrema of χ are known as the easy axes and are (i) tangential, $n_{\parallel}^*=1$, when $\chi_2<0$, and (ii) homeotropic, $n_{\perp}^*=1$, when $\chi_2>0$. Figure 5 shows the unit tangent vector $\mathbf{t}$, the director $\mathbf{n}$, the principal anisotropy axes $\mathbf{p}_o$ and $\mathbf{b}_o$, and the line vectors $\boldsymbol{\xi}$ and $-\boldsymbol{\xi}_{\perp}$ for the homeotropic ($\chi_2>0$) case. Rotation of $\mathbf{t}$ around $\mathbf{b}_o$ in the direction imposed by $-\boldsymbol{\xi}_{\perp}$ gives the fastest rate of decrease in anchoring energy, as indicated in Fig. 5 by the rotation arrow and the $\oplus$ sign, above the $\mathbf{b}_o$ axis. For the tangential case, the orientations of $\boldsymbol{\xi}_{\perp}$ and $-\boldsymbol{\xi}_{\perp}$ are reserved, since $\chi_2<0$. The torque $\boldsymbol{\sigma}$ acting on the unit tangent $\mathbf{t}$ is then given by

$$\boldsymbol{\sigma}=\boldsymbol{\xi}\times\mathbf{t}=\mathbf{t}\times(-\boldsymbol{\xi}_{\perp})=-\chi'(\mathbf{t}\times\mathbf{n}_{\perp}). \tag{22}$$

IV. EQUIVALENCE OF LINE TENSION VECTOR AND ELASTIC LINE STRESS VECTOR

The previous model of contact line nematostatics [13] is based on the elastic line stress tensor $\mathbf{T}$. This fundamental quantity defines the line tension force density $\mathbf{f}$, $\mathbf{f}=(\boldsymbol{\nabla}_{\ell}\cdot\mathbf{T})$, and the torque on the director, $\mathbf{T}_{\chi}=-\boldsymbol{\varepsilon}:\mathbf{T}$; here $\boldsymbol{\varepsilon}$ is the alternator tensor. As in the case of interfaces [21,22], we next show that an equivalent but more transparent formulation than the line stress tensor model emerges by using the line tension vector.

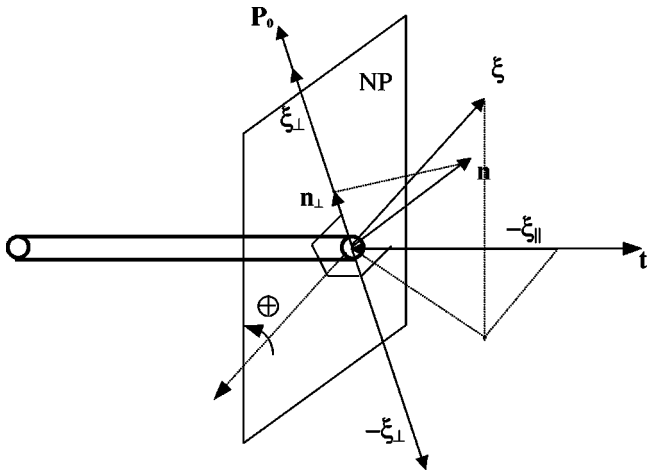

FIG. 5. Definition and geometry of the contact line vector for nematic contact lines. Schematic of the unit tangent vector **t**, the director **n**, the principal anisotropy axes $\mathbf{p}_o$ and $\mathbf{b}_o$, and the line vectors $\boldsymbol{\xi}$ and $-\boldsymbol{\xi}_\perp$ for the homeotropic case ($\chi_2>0$); in this case the preferred **n** is normal to **t**. Rotation of **t** around $\mathbf{b}_o$ in the direction imposed by $-\boldsymbol{\xi}_\perp$ gives the fastest rate of decrease in anchoring energy, as indicated by the rotation arrow and $\oplus$ sign, above the $\mathbf{b}_o$ axis. For the tangential case, the orientations of $\boldsymbol{\xi}_\perp$ and $-\boldsymbol{\xi}_\perp$ are reversed, since in this case $\chi_2<0$.

We first summarize the main features of the previously derived line stress tensor [13]. The 1×3 line stress tensor **T** contains the following normal T_n and bending T_b components:

$$\mathbf{T}=\mathbf{T}_n+\mathbf{T}_b\,. \tag{23}$$

The normal stress component $\mathbf{T}_n$ is the 1D analog to 3D bulk pressure tensor components and 2D surface tension tensor components, and accounts for line tension [8],

$$\mathbf{T}_n=+\chi\mathbf{I}_\ell\,. \tag{24}$$

The bending contribution $\mathbf{T}_b$, found from a variation due to small changes in the unit tangent vector **t**, is [13]

$$\mathbf{T}_b=\mathbf{t}(\mathbf{I}-\mathbf{tt})\cdot\frac{\partial\chi}{\partial\mathbf{t}}=\mathbf{t}(\mathbf{pp}+\mathbf{bb})\cdot\frac{\partial\chi}{\partial\mathbf{t}} \tag{25}$$

and arises because energy changes with changes in **t**. In the principal line frame (**t**,**p**,**b**), the bending stress T_b has two components [13],

$$\mathbf{T}_b=\left(\mathbf{p}\cdot\frac{\partial\chi}{\partial\mathbf{t}}\right)\mathbf{tp}+\left(\mathbf{b}\cdot\frac{\partial\chi}{\partial\mathbf{t}}\right)\mathbf{tb}. \tag{26}$$

Bending stresses take their name because they only have (**tp**) and (**tb**) components, that is, normal to the contact line. Bending stresses are found in cables, strings, ropes, filaments, and quasi-1D materials [29]. Collecting results, the total 1×3 line stress tensor is [13]

$$\mathbf{T}=T^{tt}\mathbf{tt}+T^{tp}\mathbf{tp}+T^{tb}\mathbf{tb}=\chi\mathbf{tt}+\left(\mathbf{p}\cdot\frac{\partial\chi}{\partial\mathbf{t}}\right)\mathbf{tp}+\left(\mathbf{b}\cdot\frac{\partial\chi}{\partial t}\right)\mathbf{tb}. \tag{27}$$

Next we establish the relation between the stress tensor **T** and the line tension vector $\boldsymbol{\xi}$. Comparing Eqs. (18) and (23)–(26), we find that the correspondence between the line stress tensor **T** and the line tension vector $\boldsymbol{\xi}$ is

$$\mathbf{T}=\mathbf{t}\boldsymbol{\xi}, \tag{28a}$$

$$\mathbf{T}_n=\mathbf{t}\boldsymbol{\xi}_\parallel=\chi\mathbf{tt}, \tag{28b}$$

$$\mathbf{T}_b=\mathbf{t}\boldsymbol{\xi}_\perp=\chi'\mathbf{tn}_\perp\,. \tag{28c}$$

In other words, the line tension vector is the stress vector $\mathbf{T}^v$, where $\mathbf{T}^v=\mathbf{t}\cdot\mathbf{T}=\boldsymbol{\xi}$. Thus the components of the stress tensor **T** in terms of the contact line vector $\boldsymbol{\xi}$ are

$$\mathbf{T}=(\xi^t,\xi^p,\xi^b)=(\xi_\parallel,\xi_\perp^p,\xi_\perp^b)=\left(\chi,\mathbf{p}\frac{\partial\chi}{\partial\mathbf{t}},\mathbf{b}\frac{\partial\chi}{\partial\mathbf{t}}\right). \tag{29}$$

Equation (29) establishes the correspondence between **T** and $\boldsymbol{\xi}$.

Two additional results involving the line tension vector establish its role in contact line statics. First, as mentioned above, the dual $\mathbf{T}_x$ of the line stress tensor **T**, $\mathbf{T}_x=-\boldsymbol{\varepsilon}:\mathbf{T}$, is the torque acting on the director. Introducing the line tension vector $\boldsymbol{\xi}$, we find that the torque is then

$$\mathbf{T}_x=-\boldsymbol{\varepsilon}:\mathbf{T}=\mathbf{t}\times\boldsymbol{\xi}=\mathbf{t}\times\boldsymbol{\xi}_\perp=\chi'(\mathbf{t}\times\mathbf{n}_\perp), \tag{30}$$

which shows that the torque acting on the director is equal and opposite to the torque acting on the unit tangent: $\mathbf{T}_x=-\boldsymbol{\sigma}$ [see Eq. (22)]. Secondly, in 3D nematostatics the torque balance equation is implied by the force balance equation [6]. Likewise, in 1D nematostatics the projection of the director torque balance equation along the tangent direction is implied by the force balance equation along that direction. The 1D gradient of the line energy is

$$\boldsymbol{\nabla}_\ell\chi=\frac{\partial f_\ell}{\partial\mathbf{n}}\cdot(\boldsymbol{\nabla}_\ell\mathbf{n})^T+\frac{\partial\chi}{\partial\mathbf{t}}\cdot(\boldsymbol{\nabla}_\ell\mathbf{t})^T, \tag{31}$$

where the superscript *T* denotes the transpose. Upon subtraction of the first term on the right-hand side, it becomes

$$\boldsymbol{\nabla}_\ell\chi-\frac{\partial\chi}{\partial\mathbf{t}}\cdot(\boldsymbol{\nabla}_\ell\mathbf{t})^T=\boldsymbol{\nabla}_\ell\chi-\mathbf{I}_c\cdot\frac{\partial\chi}{\partial\mathbf{t}}\cdot(\boldsymbol{\nabla}_\ell\mathbf{t})^T=\frac{\partial\chi}{\partial\mathbf{n}}\cdot(\boldsymbol{\nabla}_\ell\mathbf{n})^T. \tag{32}$$

Using equation Eqs. (6), (15b), and (17), we recognize that

$$\boldsymbol{\nabla}_\ell\chi-\frac{\partial\chi}{\partial\mathbf{t}}\cdot(\boldsymbol{\nabla}_\ell\mathbf{t})^T=\mathbf{t}\cdot\frac{\partial\boldsymbol{\xi}}{\partial s}, \tag{33}$$

finally leading to required equality

$$\mathbf{t}\cdot\frac{\partial\boldsymbol{\xi}}{\partial s}=\left(\frac{\partial f_\ell}{\partial\mathbf{n}}\right)\cdot\frac{\partial\mathbf{n}}{\partial s}. \tag{34}$$

The left-hand side is the force on the contact line [see Eqs. (36), and (37a) below] and the term in parentheses on the right-hand side is the director torque that appears in the line

torque balance equation (30). Equation (34) establishes that the force balance equation implies the torque balance equation, as in the bulk case [6].

In partial summary, we showed that the line tension vector $\boldsymbol{\xi}$ is the line stress vector $\mathbf{T}^v$, and established the correspondence between the previously formulated stress tensor model [13] and the present contact line vector formulation. The torque generated by anchoring energy on the director is equal and opposite to the torque acting on the unit tangent. The origin of the energy contributions to the line tension vector sheds light on the mechanism that generates macroscopic line stress.

V. SHAPE EQUATION FOR ANISOTROPIC CONTACT LINES AND NEMATIC CONTACT LINES

In this section, we use the line tension vector $\boldsymbol{\xi}$ to derive the governing force balance equation on a contact line, the anisotropic contact line-shape equation, and the nematic contact line-shape equation. Details of the force balance equation using the line stress model are given in [13].

The static force balance equation on anisotropic liquid crystal contact lines is given by [13]

$$\boldsymbol{\nabla}_\ell \cdot \mathbf{T}_\ell + \mathbf{F}_s + \mathbf{F}_b = \mathbf{0}, \tag{35}$$

where $\mathbf{F}_s$ is a junction sum of surface forces and $\mathbf{F}_b$ is a junction integral of long-range bulk forces. For isotropic liquids, in the absence of line and bulk forces, Eq. (35) reduces to the contact angle Young equation [8]: $\mathbf{p}\cdot\mathbf{F}_s=\mathbf{0}$. Using the equality $\mathbf{T}=\mathbf{t}\boldsymbol{\xi}$, the anisotropic contact line force balance equation (35) simplifies to

$$\frac{\partial \boldsymbol{\xi}}{\partial s} + \mathbf{F}_s + \mathbf{F}_b = \mathbf{0} \tag{36}$$

whose projection along the principal geometric frame **(t,b,p)** yields the following much simpler equations:

$$\left(\frac{\partial \xi^t}{\partial s} - \kappa \xi^p\right) + \mathbf{t}\cdot(\mathbf{F}_s + \mathbf{F}_b) = \mathbf{0}, \tag{37a}$$

$$\left(\frac{\partial \xi^p}{\partial s} + \kappa \xi^t - \tau \xi^b\right) + \mathbf{p}\cdot(\mathbf{F}_s + \mathbf{F}_b) = \mathbf{0}, \tag{37b}$$

$$\left(\frac{\partial \xi^b}{\partial s} + \tau \xi^p\right) + \mathbf{b}\cdot(\mathbf{F}_s + \mathbf{F}_b) = \mathbf{0}, \tag{37c}$$

where (ξ^t, ξ^p, ξ^b) are defined in Eq. (29). Equations (37) are consistent with the classical force equations for rods, strings, filaments, and cables [29]. Equations (37b) and (37c) are the shape equation for anisotropic contact lines, since they govern the curvature κ and twist τ of the line. For the current constitutive Eq. (15b) there is no torsion energy associated with the contact line [see Eqs. (15)] and hence Eqs. (37) simplify to

$$f_t + \mathbf{t}\cdot(\mathbf{F}_s + \mathbf{F}_b) = \mathbf{0}, \tag{38a}$$

$$f_t = \frac{\partial \chi_o}{\partial s}, \tag{38b}$$

$$f_p + \mathbf{p}\cdot(\mathbf{F}_s + \mathbf{F}_b) = \mathbf{0}, \tag{38c}$$

$$f_p = \frac{\partial \mathbf{n}}{\partial s}\cdot\frac{\partial \xi^p}{\partial \mathbf{n}} + \kappa\{\chi + \chi''[(\mathbf{n}\cdot\mathbf{p})^2 - (\mathbf{n}\cdot\mathbf{t})^2]\}, \tag{38d}$$

$$f_b + \mathbf{b}\cdot(\mathbf{F}_s + \mathbf{F}_b) = \mathbf{0}, \tag{38e}$$

$$f_b = \left(\frac{\partial \mathbf{n}}{\partial s}\cdot\frac{\partial \xi^b}{\partial \mathbf{n}} + \kappa\chi''(\mathbf{nn}:\mathbf{pb})\right), \tag{38f}$$

where $f_i;\ i=t,p,b$, are the magnitudes of tangential, bending, and twisting forces acting on the contact line, respectively, and where $\chi''=\chi_2$. Clearly line tension anisotropy renormalizes the effect of the line tension χ on the curvature force. Equation (38d) shows that the effective line tension χ_{eff} in the presence of anisotropy depends on nematic orientation with respect to the contact line: $\chi_{\text{eff}}=\chi+\chi''[(\mathbf{n}\cdot\mathbf{p})^2 - (\mathbf{n}\cdot\mathbf{t})^2]$. In addition, the 1D shape equation (38d) shows that line gradients of the orientation give rise to new curvature- and torsion-independent contributions. For isotropic contact lines, Eqs. (38) simplify to

$$\frac{\partial \chi_o}{\partial s} = 0, \quad \kappa\chi_o + \mathbf{p}\cdot\mathbf{F}_s = \mathbf{0}, \quad \mathbf{b}\cdot\mathbf{F}_s = 0. \tag{39}$$

The **p** component of the force balance equations (38c) and (38d) is the line-shape equation, since it governs its curvature, and is the 1D analog to the 2D nematic Herring equation for anisotropic surfaces [30], given in Eq. (5). A more revealing expression of Eq. (38d) is obtained by separating and identifying the physical mechanism that can change the shape of the line. The three mechanisms contributing to the bending force f_p are

$$f_p = \underbrace{\kappa\chi}_{\text{line length}} + \underbrace{\kappa\chi''[(\mathbf{n}\cdot\mathbf{p})^2 - (\mathbf{n}\cdot\mathbf{t})^2]}_{\text{line orientation}} + \underbrace{\frac{\partial \mathbf{n}}{\partial s}\cdot\frac{\partial \xi^p}{\partial \mathbf{n}}}_{\text{director curvature}}, \tag{40}$$

which shows that bending forces are generated by the contact line length, the contact line orientation, and director gradients. The correspondence between the contact line and the interface shape equations is

	Interface	Contact Line
tension	γ	χ
anisotropic effect	γ''	χ''
geometric vectors	e_i, $\mathbf{k}$	$\mathbf{p}$, $\mathbf{t}$
effect	$-p_c$	f_p
shape equation	(5)	(40)

where all symbols have been previously defined. The bending force f_p acting on the contact line is the 1D analog of the capillary pressure $-p_c$ across the interface.

For straight contact lines ($\kappa=0$), the only bending force is generated by director curvature,

$$f_p=\frac{\partial \mathbf{n}}{\partial s}\cdot\frac{\partial \xi^p}{\partial \mathbf{n}}=\chi''\left\{\mathbf{n}\cdot(\mathbf{tp}+\mathbf{pt})\cdot\frac{\partial \mathbf{n}}{\partial s}\right\}. \tag{41}$$

For curved contact lines and director orientation along the principal axis, say $\mathbf{n}=\mathbf{p}$, the bending force f_p is

$$f_p=\kappa\chi_0, \tag{42}$$

as in an isotropic contact line. For curved contact lines and orientation along the unit tangent, $\mathbf{n}=\mathbf{t}$,

$$f_p=\kappa\left(\chi_0-\frac{\chi_2}{2}\right), \tag{43}$$

and the bending force is renormalized by the anchoring energy. Since the sign of χ_2 is undetermined, competition or cooperation between contraction and tilting of the contact line may result.

In partial summary, the shape equations (38c) and (38d) for anisotropic contact lines are the 1D analog of the 2D capillary pressure Herring equation (1) for anisotropic surfaces [30]. Bending forces in anisotropic liquid-crystal contact lines include a number of novel effects: (a) bending forces even for straight contact lines, (b) orientation-dependent renormalization of the line tension coefficents due to anchoring energy, and (c) bending forces due to orientation curvature. We next analyze the stability of nematic-liquid-crystal contact lines, where the manifestations of these novel phenomena clearly emerge.

VI. APPLICATION OF LINE VECTOR THERMODYNAMICS: ANCHORING-DRIVEN SHAPE TRANSITIONS IN NEMATIC CONTACT LINES

In this section, we use the new formalism to analyze linear instabilities of the straight nematic contact line driven by changes in anchoring energy. These changes may arise due to changes in temperature or concentration. The spirit of the presentation is to provide an example of the utility of the contact line vector approach. We realize that a complete and rigorous solution to nematic contact line problems involves the simultaneous solution of bulk, interfaces, and line equations [13], which is beyond the scope of this work.

We assume that $\mathbf{n}$ is given and constant and the soft contact line changes conformation due to changes in the anchoring energy. The amplitude of the conformational change is infinitesimal since we consider linear instabilities. The scaled bending force that determines the shape of the line is, from Eq. (40),

$$\overline{f_p}\equiv f_p/\chi_0=\kappa\{1+W[(\mathbf{n}\cdot\mathbf{p})^2-\tfrac{1}{2}(\mathbf{n}\cdot\mathbf{t})^2]\}, \tag{44a}$$

$$W=\frac{\chi_2}{\chi_0}. \tag{44b}$$

The instability threshold condition for deviations from a straight line ($\kappa=0$) configuration is then

$$\overline{f}^*=\kappa\{1+W[(\mathbf{n}\cdot\mathbf{p})^2-\tfrac{1}{2}(\mathbf{n}\cdot\mathbf{t})^2]\}\geqslant 0, \tag{45}$$

where we dropped the p subscript for convenience. Thus the contact line conformation depends on geometry κ and orientation $\mathbf{n}$. The four characteristic small amplitude line fluctuation modes are (a) bending-tangential (BT) mode, (b) bending-homeotropic (BH), (c) helical-tangential (HT), and (d) helical-homeotropic (HH), discussed below; it is noted that bending and helical refer to the geometry of the mode while tangential and homeotropic refer to the director orientation $\mathbf{n}$ with respect to the unit tangent $\mathbf{t}$.

A. Bending modes

The bending or sinusoidal mode is planar and the line is confined to a plane, say $x-z$. In a rectangular coordinate system, assuming a small harmonic perturbation of amplitude a and wave vector η on a contact line along the z axis, the line equation, the unit tangent vector $\mathbf{t}$, the principal unit normal vector $\mathbf{p}$, and the curvature κ are given by

$$\mathbf{r}=[a\cos(\eta z),0,z)], \tag{46a}$$

$$\mathbf{t}=[-ak\sin(\eta z),0,1)], \tag{46b}$$

$$\mathbf{p}=[1,0,a\eta\sin(\eta z)], \tag{46c}$$

$$\kappa=-a\eta^2\sin(\eta z). \tag{46d}$$

(a) Bending-tangential (BT) mode. For tangential orientation $\mathbf{n}=(0,0,1)$, the threshold equation gives

$$\overline{f}^*_{\mathrm{bt}}=-a\eta^2\sin(\eta z)\left\{1-\frac{W}{2}\right\}\geqslant 0. \tag{47}$$

Thus a bending-tangential mode emerges when $W>2$.

(b) Bending-hometropic (BH) mode. For homeotropic orientation $\mathbf{n}=(1,0,0)$, the threshold equation gives

$$\overline{f}^*_{\mathrm{bh}}=-a\eta^2\sin(\eta z)\{1+W\}\geqslant 0. \tag{48}$$

Thus a bending-homeotropic mode emerges when $-2<W<-1$.

B. Helical modes

The helical mode is nonplanar and the line is confined to the surface of a cylinder of radius a. In a rectangular coordinate system, the helical contact line parametrization $\mathbf{r}(s)$, the unit tangent vector $\mathbf{t}$, the principal unit normal vector $\mathbf{p}$, and the curvature κ are given by

$$\mathbf{r}=\left(a\cos\frac{s}{c},-a\sin\frac{s}{c},\frac{bs}{c}\right), \tag{49a}$$

$$c=\sqrt{a^2+b^2},$$

$$\mathbf{t}=\left(-\frac{a}{c}\sin\frac{s}{c},-\frac{a}{c}\cos\frac{s}{c},\frac{b}{c}\right),$$
$$\mathbf{p}=\left(-\cos\frac{s}{c},+\sin\frac{s}{c},0\right),\quad \kappa=-\frac{a}{c^2}. \tag{49b}$$

The limit of a straight line appears as $a\to 0$, $c\to b$, and $\kappa\to 0$. The magnitude of b is the pitch of the helix.

(a) Helical-tangential (HT) mode. For tangential orientation $\mathbf{n}=(0,0,1)$, the threshold equation gives

$$\overline{f}^{*}_{\mathrm{ht}}=-\frac{a}{c^2}\left\{1-\frac{W}{2}\left(\frac{b}{c}\right)^2\right\}\geqslant 0. \tag{50}$$

Thus the helical-tangential mode emerges when $W>2(c/b)^2$. As $a\to 0$, this threshold converges to the threshold of bending-tangential mode: $W>2$.

(b) helical-hometropic (HH) mode. For tangential orientation without loss of generality, we take $\mathbf{n}=(1,0,0)$, and the threshold equation gives

$$(\mathbf{n}\cdot\mathbf{t})^2=\left(\frac{a}{c}\right)^2\left(\sin\frac{s}{c}\right)^2, \tag{51a}$$

$$(\mathbf{n}\cdot\mathbf{p})^2=\left(\cos\frac{s}{c}\right)^2, \tag{51b}$$

$$\overline{f}^{*}_{\mathrm{hh}}=-\frac{a}{c^2}\left\{1+W\left[\left(\cos\frac{s}{c}\right)^2-\frac{1}{2}\left(\frac{a}{c}\right)^2\left(\sin\frac{s}{c}\right)^2\right]\right\}\geqslant 0. \tag{51c}$$

Thus the helical-tangential mode emerges when

$$W<\frac{-1}{\left[\cos\left(\frac{s}{c}\right)\right]^2-\frac{1}{2}\left(\frac{a}{c}\right)^2\left[\sin\left(\frac{s}{c}\right)\right]^2}. \tag{52}$$

In the limit of infinitesimal helix radius $(a\to 0)$, the inequality becomes

$$W<\frac{-1}{\left(\cos\frac{s}{c}\right)^2} \tag{53}$$

and the relevant upper value is $W<-1$, which agrees with the bending-homeotropic case.

Figure 6 shows the contact line-shape phase diagram in terms of the dimensionless anchoring energy W as a function of helix aspect ratio c/b. The sinusoidal curves represent the bending modes, while the helical curves represent the helical modes. We recall that in this analysis $\mathbf{n}$ is given and constant. The straight line is defined by $c/b=1$ (i.e, $a=0$, $\kappa=0$). The contact line conformation diagram is divided into three sectors whose boundaries are obtained from Eqs. (47), (48), (50), and (52). Within the upper (half-parabola) sector, the straight contact line is unstable and the bending and helix modes are stable. Within the lower (rectangle) sector, the straight contact line is unstable and the bending and helix modes are stable. For tangential director orientation (the $W>0$ sector), the bending-tangential (BT) and helical-tangential (HT) modes set in for $W>2$. The smaller the pitch, the higher the value of the required anchoring constant (W) necessary to find the HT mode. Likewise, when the director is normal to the line and $W<-1$, the bending-homeotropic (BH) and helical-homeotropic (HH) modes set in. In the linear regime, the critical value of W for helical-homeotropic distortions is independent of the pitch. As the pitch decreases, additional energies have to be taken into account to regularize this Haddamard-like instability. Good candidates are higher-order bending corrections [31] and surface and bulk forces acting on the line [13], but their exact treatment is beyond the scope of this paper.

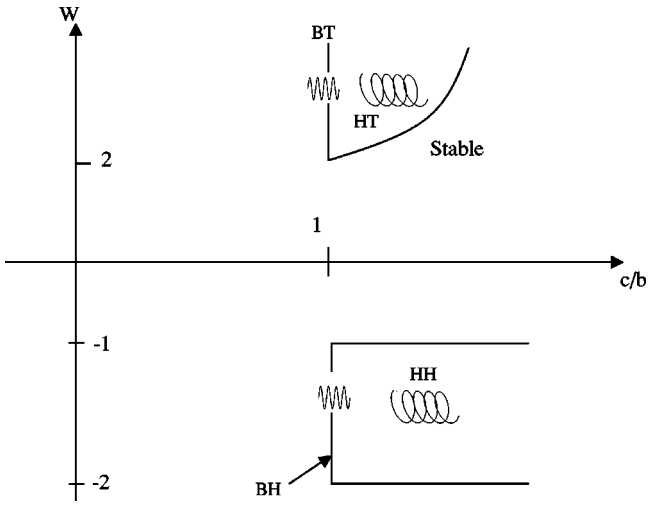

FIG. 6. Nematic contact line-shape phase diagram in terms of the dimensionless anchoring energy W as a function of helix aspect ratio c/b. The sinusoidal curve represents the bending modes, while the helical curve represents the helical modes. The straight line is defined by $c/b=1$ (i.e., $a=0$, $\kappa=0$). For tangential orientation ($W>0$ sector), the bending-tangential (BT) and helical-tangential (HT) modes set in for $W>2$. The smaller the pitch, the higher the value of the required anchoring constant (W) necessary to find the HT mode. Likewise, when the director is normal to the line and $-2<W<-1$, the bending-homeotropic (BH) and helical-homeotropic (HH) modes set in. In the linear regime, the critical value of W for helical-homeotropic distortions is independent of the pitch.

VII. CONCLUSIONS

Line tension vector thermodynamics provides a clear pathway to analyze contact line problems in the presence of anisotropy by differentiating the two possible elastic modes, namely change in contact line length and change in contact line orientation [Eqs. (15b) and (15c)]. The equivalence of contact line vector thermodynamics and the equations of 1D nematostatics were established [Eq. (28)]. The 1D shape equation [Eq. (40)] shows that anisotropy renormalizes the line tension coefficient with a term that depends on the cur-

vature of line tension in orientation space [Eq. (40)]. An application of the shape equation to analyze shape transitions driven by anchoring energies (Fig. 6) shows that the line vector thermodynamics is a useful tool to analyze the role of anisotropy in contact line processes.

ACKNOWLEDGMENTS

This work is supported by a grant from the Donors of The Petroleum Research Fund (PRF) administered by the American Chemical Society.

[1] A.A. Sonin, *The Surface Physics of Liquid Crystals* (Gordon and Breach, Amsterdam, 1995).
[2] B. Jerome, *Surface Alignment*, in *Handbook of Liquid Crystals*, edited by D. Demus, J. Goodby, G.W. Gray, H.-W. Spiess, and V. Vill (Wiley-VCH, Weinheim, 1998), Vol. 1.
[3] H. Yokoyama, *Handbook of Liquid Crystal Research*, edited by P.J. Collins and J.S. Patel (Oxford University Press, New York, 1997), Chap. 6, p. 179.
[4] T.J. Sluckin and A. Poniewierski, in *Fluid Interfacial Phenomena*, edited by C.A. Croxton (Wiley, Chichester, 1986), Chap. 5.
[5] M.A. Osipov and S. Hess, J. Chem. Phys. **99**, 4181 (1993).
[6] E.G. Virga, *Variational Theories for Liquid Crystals* (Chapman Hall, London, 1994).
[7] G. Barbero and G. Durand, in *Liquid Crystals in Complex Geometries*, edited by G.P. Crawford and S. Zumer (Taylor and Francis, London, 1996), p. 21.
[8] D.A. Edwards, H. Brenner, and D.T. Wasan, *Interfacial Transport Processes and Rheology* (Butterworth, Stoneham, MA, 1991).
[9] J.C. Slattery, *Interfacial Transport Phenomena* (Springer-Verlag, New York, 1990).
[10] A. Poniewierski, Liq. Cryst. **27**, 1369 (2000).
[11] A.D. Rey, Phys. Rev. E **61**, 1540 (2000).
[12] A.D. Rey, J. Chem. Phys. **110**, 9769 (1999).
[13] A.D. Rey, Phys. Rev. E **67**, 011706 (2003).
[14] P.G. de Gennes and J. Prost, *The Physics of Liquid Crystals*, 2nd ed. (Oxford University Press, London, 1993).
[15] A.D. Rey, Liq. Cryst. **28**, 549 (2001).
[16] A.K. Sen and D.E. Sullivan, Phys. Rev. A **35**, 1391 (1987).
[17] E.F. Gramsbergen, L. Longa, and W.H. de Jeu, Phys. Rep. **135**, 195 (1986).
[18] J.T. Jenkins and P.J. Barrat, Q. J. Mech. Appl. Math. **27**, 111 (1974).
[19] D.W. Hoffman and J.W. Cahn, Surf. Sci. **31**, 368 (1972).
[20] J.W. Cahn and D.W. Hoffman, Acta Metall. **22**, 1205 (1974).
[21] A.G. Cheong and A.D. Rey, J. Chem. Phys. **117**, 5062 (2002).
[22] A.-G. Cheong and A.D. Rey, Phys. Rev. E **66**, 021704 (2002).
[23] U. Gehlert, G. Weidemann, and D. Vollhardt, J. Colloid Interface Sci. **392**, 174 (1995).
[24] D. Pettey and T.C. Lubenski, Phys. Rev. E **59**, 1834 (1999).
[25] A.H. King, Interface Sci. **7**, 251 (1999).
[26] W.W. Pai and J. Wendelken, Phys. Rev. Lett. **86**, 3088 (2001).
[27] A.I. Rusanov, Colloids Surf., A **156**, 315 (1999).
[28] D.R. Nelson, *Defects and Geometry* (Cambridge University Press, Cambridge, 2002).
[29] P. Villagio, *Mathematical Models for Elastic Structures* (Cambridge University Press, New York, 1997).
[30] A.P. Sutton and B.W. Balluffi, *Interfaces in Crystalline Materials* (Oxford Science Publication, Clarendom Press, New York, 1996).
[31] A.G. Cheong and A.D. Rey, Eur. Phys. J. E **9**, 171 (2002).